Building and Environment 223 (2022) 109438

Contents lists available at ScienceDirect

Building and Environment

journal homepage: www.elsevier.com/locate/buildenv

Effects of thermal comfort-driven control based on real-time clothing insulation estimated using an image-processing model

Eun Ji Choi, Bo Rang Park, Nam Hyeon Kim, Jin Woo Moon *

School of Architecture and Building Science, Chung-Ang University, 84, Heukseok-ro, Dongjak-gu, Seoul, 06974, South Korea

ARTICLE INFO

Keywords:
Thermal comfort
Predicted mean vote
Clothing insulation
Occupant-centric control
Image processing model

ABSTRACT

The aim of this study is to estimate real-time clothing insulation (R-CLO) and to evaluate the effectiveness of predicted mean vote (PMV)-based control on thermal comfort and electrical energy. For this purpose, an image-processing R-CLO model was developed to estimate the clothing insulation for various ensembles of garments worn by the occupants. The R-CLO model classified 16 individual garments and estimated the total clothing insulation for various ensembles based on these garments. Performance testing using the PMV output from the R-CLO model was conducted. The resulting PMV-based control changed the indoor set temperature according to changes in the clothing insulation, which improved the thermal comfort of the occupants when compared with existing control methods. Even though the proposed control method established a comfortable indoor environment for all clothing conditions, but also affected the electrical energy. The electrical energy is increased as the clothing insulation increased. This study confirmed the potential of comfort-driven control using a vision-based R-CLO model and verified that actual clothing information is required to achieve thermal comfort in the real building as well as to operate the system considering energy.

1. Introduction

1.1. Background

A number of factors determine the quality of an indoor environment, with thermal quality in particular determining the thermal comfort of the occupants, which has an important influence on their health, work productivity [1,2], and quality of life [3–5]. Because thermal comfort is considered important in terms of architecture, including the optimal control of building surfaces and facility systems, a number of previous studies have sought to improve thermal comfort using experiments and simulations [6–8]. To evaluate the thermal comfort of occupants, personal factors such as their metabolic rate and clothing insulation and environmental factors such as air temperature, relative humidity, mean radiant temperature, and air velocity have been considered. Based on these factors, various models have been developed to evaluate thermal comfort [9,10], including the predicted mean vote (PMV) [10], which is a thermal comfort index used in international standards such as ISO 7730 [11], ASHRAE Standard 55 [12], and CEN 15251 [13] that quantifies thermal comfort based on both environmental and personal factors.

Despite the previous research on thermal comfort, if occupants information such as their activity patterns and preferences are not considered when operating a building, an uncomfortable environment can be created and inefficient operating decisions can be made that lead to unnecessary energy consumption [14,15]. As such, for the optimal operation of a building, the two-way interaction between the occupants and the building must be considered. Recently, occupant-centric control, which aims to improve thermal comfort and reduce energy consumption by considering occupant information, has emerged as a new research field [14,16,17]. In particular, the introduction of deep learning technologies capable of pattern recognition, data mining, and image processing for complex data and of hardware technologies such as the Internet of Things [16,18] and advanced sensing devices [19–21] has led to the development of data-based models and new approaches to occupant-centric building control [7,14,22–24].

Clothing insulation and the metabolic rate are occupant characteristics that are particularly important in determining thermal comfort, and a building should be operated considering the actual thermal comfort of the occupants. Therefore, comfort-driven building control using PMV indicators has been employed to create a comfortable environment customized to the occupants. In this approach, unlike with general dry-bulb temperature (DBT)-based control, complex thermal

* Corresponding author.
E-mail addresses: ejjchl77@cau.ac.kr (E.J. Choi), pbr_1123@naver.com (B.R. Park), skagus1546@cau.ac.kr (N.H. Kim), gilerbert73@cau.ac.kr (J.W. Moon).

https://doi.org/10.1016/j.buildenv.2022.109438
Received 3 May 2022; Received in revised form 12 July 2022; Accepted 19 July 2022
Available online 3 August 2022

Nomenclature

T_a	air temperature [°C]
V_a	air velocity [m/s]
I_{cl}	clothing insulation [clo or m^2 ˙K/W]
I_{clu}	garment insulation [clo or m^2 ˙K/W]
T_r	mean radiant temperature [°C]
M	metabolic rate [met or W/m^2]
T_o	operative temperature [°C]
PMV	predicted mean vote
RH	relative humidity [%]
TSV	thermal sensation vote
TSVr	relative thermal sensation
R-CLO	real-time clothing insulation
DBT	dry-bulb temperature

environment factors are considered. However, the personal factors that determine the PMV are dynamic in a real environment, which is difficult to measure or predict using sensors. Therefore, personal factors are usually assumed to be fixed values for calculating PMV [25,26]. For this reason, even if the PMV is used as a control variable in conventional building control, the actual thermal comfort of the occupants is not taken into account.

On/off control based on a simple indoor set temperature or PMV-based control using fixed personal factors have been widely employed in existing building control systems. To use PMV as an accurate control variable, a method for obtaining comfort information based on occupant characteristics such as their metabolic rate and clothing insulation is required [27,28]. Clothing insulation is a dynamic variable that is determined by social and psychological factors, meaning that field-based measurements must be taken to effectively employ it in a control system. However, due to the absence of sensors and methods that can be used to effectively measure clothing insulation, various models are being developed, including traditional data-driven methods, machine learning including artificial intelligence-based methods such as deep learning using thermal imaging and RGB cameras.

1.2. Clothing insulation measurement methods

Clothing insulation (I_{cl}) is defined as the insulation provided by all of the clothing worn by a person, representing the thermal resistance between the skin and the surface of the clothing (1.0 clo = 0.155 m^2K/W) [12]. The type, material, and thickness of individual garments determine the clothing insulation of the overall ensemble, thus it is a dynamic variable that varies depending on the garment. ISO 9920 [29] and ASHRAE Standard 55 [12] provide standards for general garments and ensembles, specifying types, materials, and clothing insulation values. Accurate measurements of clothing insulation require expensive equipment, such as thermal mannequins and climate chambers capable of precise thermal environmental control [30,31]. However, it is impossible to measure the real-time insulation for the numerous ensembles that may occur within a building environment in this manner. For this reason, when calculating thermal comfort, fixed values of 0.5 clo in summer and 1.0 clo in winter [12,32] or direct survey approaches [5,33,34] have generally been employed.

However, in the field, control systems based on thermal comfort must be operated by measuring the dynamic clothing insulation of the occupants without their direct participation. To solve this problem, various studies have sought to develop data-driven and/or sensor-based models that can indirectly determine the clothing insulation of the occupants. Data-driven models employ field survey data and environmental variables that can be measured by sensors, with regression or logistic models employed to predict the average daily clothing insulation based on its correlation with key environmental variables, including the highest and average outdoor temperature [33,35] and the outdoor temperature at 6 a.m. [36,37]. However, when using only environmental variables to predict clothing insulation, there are limitations associated with the diversity of regional and climatic data and differences in customary, psychological, and individual fashion preferences. In addition, because the daily average clothing insulation does not consider hourly clothing information, it is difficult to effectively ensure thermal comfort using a building control system.

To overcome these limitations of data-driven models, measurement-based clothing insulation models using invasive or noninvasive sensors in wearable devices, thermal cameras, and RGB cameras, have been proposed. Thermal cameras have the ability to measure the skin and clothing surface temperature to predict real-time clothing insulation [38,39]. Miura et al. [38] used a thermal camera and thermal depth images to measure the clothing and skin surface temperature and calculate the clothing insulation. Lee et al. [39] also proposed a method for calculating clothing insulation for winter, spring/autumn, and summer by measuring the temperature of exposed skin on the forehead, chest, and legs using a thermal camera. These approaches can calculate clothing insulation without direct occupant participation using noninvasive sensors, but infrared (IR) cameras can be inaccurate in practice depending on the distance to the measurement target, and only exposed body parts can be measured using the sensors [17].

Another approach for measuring real-time clothing insulation is the use of RGB images as input to image-processing models based on deep learning architecture that estimate clothing insulation by classifying the types of garment worn by the occupants [27,40,41]. Dziedzic et al. [42] developed a new measurement technique that quantifies the coefficients for clothing insulation using depth and RGB images taken from a Kinect device. They confirmed the potential of detecting the patterns of three types of ensembles and the detection accuracy was 74.29%, which requires further improvement. Matsumoto et al. [41] developed a model that calculates clothing insulation using image-based machine learning that estimated the weight of individual clothes, from which the PMV can be calculated. The PMV estimation error was demonstrated to be lower than that calculated by the fixed clothing insulation value. Liu et al. [27] presented an approach to measuring clothing insulation and the metabolic rate using a vision-based technique. They developed a model that provided an input source using a thermal camera and recognized clothing types using a convolutional neural network (CNN) structure. Basic clothing insulation was estimated by measuring the skin and clothing temperature, and classification was carried out for five types of tops only (long sleeves, long sleeves with unzipped sleeves, roll-up sleeves, roll-up sleeves with unzipped sleeves, and T-shirts). Choi et al. [40] developed a model framework that classified five clothing ensembles in real-time using an image processing-based deep learning model, producing an accuracy of 86% in a real environment. In addition, they demonstrated that a PMV-based control system based on the model improved the thermal comfort of the occupants.

1.3. Research purpose and process

Previous studies have confirmed the potential utility of estimating clothing insulation based on images in order to create a more comfortable environment in consideration of actual clothing information. However, previous models have tended to classify only a few types of garments or a few fixed clothing ensembles, meaning that they cannot effectively represent the clothing insulation in an actual building environment. Thus, because the clothing ensemble of occupants can vary dynamically, a practical approach to deciding the clothing insulation of various ensembles based on recognizing individual garments is necessary. In addition, because managing a building environment based on the comfort of the occupants can also affect the building's energy consumption [17,43–45], it is necessary to analyze the effect of building control based on clothing insulation on occupant comfort and energy

consumption.

The purpose of this study is to develop a vision-based real-time clothing insulation estimation model (hereafter referred to as the R-CLO model) for indoor environments and to evaluate the effect of PMV-based building control that considers actual clothing insulation on thermal comfort and energy consumption. The proposed R-CLO model can classify 16 individual garments and estimate the insulation of various clothing ensembles consisting of different combinations of tops and bottoms based on the classified garments. In addition, an algorithm for determining the clothing insulation representing the control cycle is developed for use in a PMV-based control system. The experiment results are analyzed in terms of thermal comfort and electrical energy consumption compared to conventional control methods.

In this study, an experiment was conducted on a single occupant during the cooling season in four major stages (Fig. 1). In the first stage, an R-CLO model was developed to estimate the insulation of clothing ensembles based on input images, and a clothing insulation decision algorithm was created to determine the clothing insulation for a certain period that can be applied to building control. To develop the model, image datasets depicting various clothing ensembles were trained using a deep learning-based image processing network. In the second stage, the performance of the proposed model was assessed in both a test dataset and in a real environment. In the third stage, a PMV-based control system based on the proposed model was developed to reflect the clothing insulation of a subject, and comparative analysis was conducted with two conventional control methods, DBT control and PMV-based control with fixed clothing insulation (0.5 clo). The experimental results for the thermal environment, occupant thermal comfort (the PMV and thermal sensation vote (TSV)), and electrical energy in cooling mode were analyzed in terms of electricity consumption for the different control methods.

2. Methods

2.1. Real-time clothing insulation (I_{cl}) estimation model (R-CLO model)

In this study, the R-CLO model was proposed to improve an existing model developed by this research team [46]. The R-CLO model can estimate the clothing insulation (I_{cl}) for an entire clothing ensemble by detecting and classifying individual garments from images. This represents an advance on previous models, which have typically classified only top garments [27,38] or handled only a few clothing ensembles with fixed top and bottom combinations [40]. Whit these approaches, it is difficult to recognize the variety of ensembles that can occur in a real environment. For example, a model that can only classify a "T-shirt and walking shorts" ensemble needs to be retrained for a "T-shirt and long pants" ensemble. Therefore, a genuinely practical model needs to be able to autonomously estimate the overall I_{cl} by recognizing individual garments. The proposed model detects individual garments worn by a person in an image using the categories of top, bottom, outer, dress, and pajamas, and it calculates the total I_{cl} based on the detected garments. In addition, this study aims to overcome the limitations of existing control systems for the thermal environment by proposing a I_{cl} decision algorithm that determines the representative I_{cl} for a specific control period.

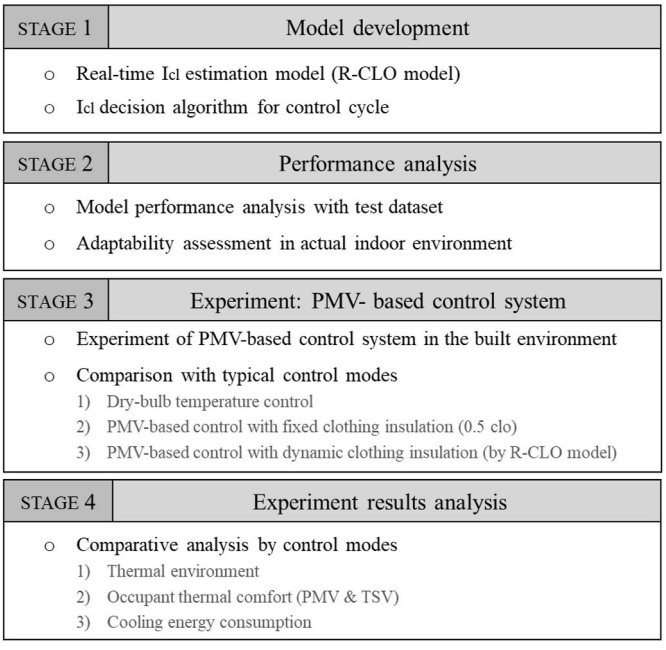

Fig. 1. Research process for the present study.

2.1.1. Dataset for training the R-CLO model

Clothing images of both individual garments and ensembles were collected to train the R-CLO model. These images contained 16 representative garments associated with the typical clothing ensembles presented in ISO 9920 [29] and ASHRAE Standard 55 [12]. The selected garments are universally worn in various types of building, including residential and office buildings. Table 1 summarizes the fiber and corresponding garment insulation (I_{clu}) for the 16 selected garments organized into five categories (top, bottom, outer, dress, and pajamas).

Image data for model training were directly collected from online and offline sources and included images depicting clothes only and those of people wearing clothes. In addition, for full-body images, the combination of garments differed so that various clothing ensembles could be trained. Images were collected for various angles (e.g., from the front, side, and rear) and poses (e.g., sitting and standing). A total of 6664 collected images were randomly divided into training (70%), validation (10%), and test (20%) datasets.

2.1.2. R-CLO model implementation

The R-CLO model was trained using the YOLO (You Only Look Once) version 5 [47] structure, which can simultaneously perform object detection and classification based on a CNN. YOLOv5 is a deep learning network algorithm for real-time object detection that trains two-dimensional data such as images or videos. It can detect and classify objects in images and offers faster image processing than other models. The backbone of YOLOv5 extracts a feature map from an image and

Table 1
Information for the 16 selected garments.

Category	Garment	I_{clu} [clo]	Fiber
Top	Short-sleeve shirt	0.24	Cotton
	Long-sleeve shirt	0.33	Cotton
	T-shirt	0.10	Cotton
	Long-sleeve sweater	0.36	85% wool, 15% nylon
	Long-sleeve sweatshirt	0.16	Cotton, wool
Bottom	Trousers (straight, loose)	0.22	Cotton
	Knee-length skirt	0.14	100% cotton
	Ankle-length skirt	0.23	100% cotton
	Walking shorts	0.08	100% cotton
	Sweatpants	0.28	50% polyester, 38% cotton, 12% viscose
Outer	Suit jacket	0.36	100% cotton
Dress	Short-sleeve shirtdress	0.29	65% polyester, 35% cotton
	Long-sleeve shirtdress	0.35	65% polyester, 35% cotton
Pajamas	Long-sleeve pajama top	0.31	65% polyester, 35% cotton
	Short-sleeve pajama top	0.25	65% polyester, 35% cotton
	Pajama trousers	0.17	65% polyester, 35% cotton

divides it into S, M, L, and XL according to the structure. In this study, the L structure was used for training, which is capable of processing images every 15 s. Based on the trained backbone information, the head detects and classifies the target object. The garment detected by the model is displayed in the image with a bounding box containing only the clothes, and the garment classification results are labeled within the bounding box.

The system platform used to implement the model was an NVIDIA Quadro RTX 8000, Ubuntu 20.04 LTS, Python 3.9.0, CUDA 11.4, and PyTorch 1.8.1. Model training was conducted using transfer learning for the pretrained model, and the model was trained with an image size of 416, a batch size of 16, and 150 epochs using the training dataset. During training, the optimizer employed stochastic gradient descent, and the learning rate and momentum were 0.02 and 0.94, respectively.

The performance of the trained model was first evaluated using the test dataset and then in a real environment. In this second assessment, an experiment was performed on subjects in a test bed, with the classification performance for the garments using the optimal model analyzed and major sources of error identified. To evaluate model performance, precision and recall were calculated, and the classification performance of each garment was confirmed using a confusion matrix. The accuracy of clothing detection from the images was then evaluated using average precision (AP), which was determined by calculating the area of the precision−recall curve using the overlapping area between the ground-truth bounding box and the output bounding box for the model as a threshold. The closer AP is to 1, the better the performance. For the multi-class model, the mean average precision (mAP) for all classes was employed.

2.1.3. Estimation process for clothing insulation (I_{cl})

To employ the R-CLO model in actual building control, it was necessary to determine the I_{cl} for the occupants for a particular control period. As outlined in Fig. 2, an I_{cl} decision algorithm was developed for this purpose that implemented the results from R-CLO model. First, indoor images were collected in 15-s cycles and employed as input data for the developed R-CLO model. The R-CLO model consequently detected and classified individual garments from the accumulated images in real-time. Based on this information, the combination of clothes classified with the highest frequency during a control cycle (10 min) was determined, and I_{cl} was calculated accordingly using Eq. (1) from ISO 9920 [29]. This method is widely used to calculate I_{cl} when the actual measurement of I_{cl} is not possible [48,49].

$$I_{cl} = 0.161 + 0.835 \sum I_{clu} \quad (1)$$

In this experiment, the I_{cl} of an occupant representing the control period was determined using the I_{cl} decision algorithm, and the indoor environment was controlled based on this real-time I_{cl}. The performance of the I_{cl} decision algorithm was evaluated for nine ensembles (see Section 2.3.3) using the mean square error between the actual and calculated I_{cl}. The results for this are summarized in Section 3.2.2.

2.2. Control methods

In this experiment, three feedback control modes were tested, labeled Modes A, B, and C. As shown in the diagram of Fig. 3, an IR sensor was employed as an actuator to send a signal of air temperature, which was determined by the controller using the built-in algorithm, to create the environment for the test bed. At this time, the control variable was set according to the control mode, and the set point, feedback elements, and feedback signal were changed in accordance with the control variable. The information for each element of the three control modes tested in this experiment is presented in Fig. 3. The control cycle was set to 10 min during the experiment.

Mode A was DBT-based control, for which the control variable was indoor air temperature. Because this experiment was conducted during the cooling period, the set point for Mode A was 25 °C. The feedback elements and feedback signal returned the measured indoor air temperature. For Modes B and C, the control variable was the PMV and the set point was PMV = 0 (i.e., a neutral state). Modes B and C transmitted the difference between the set point and the feedback PMV as an error signal. The manipulated variable was the value of T_a that produced a

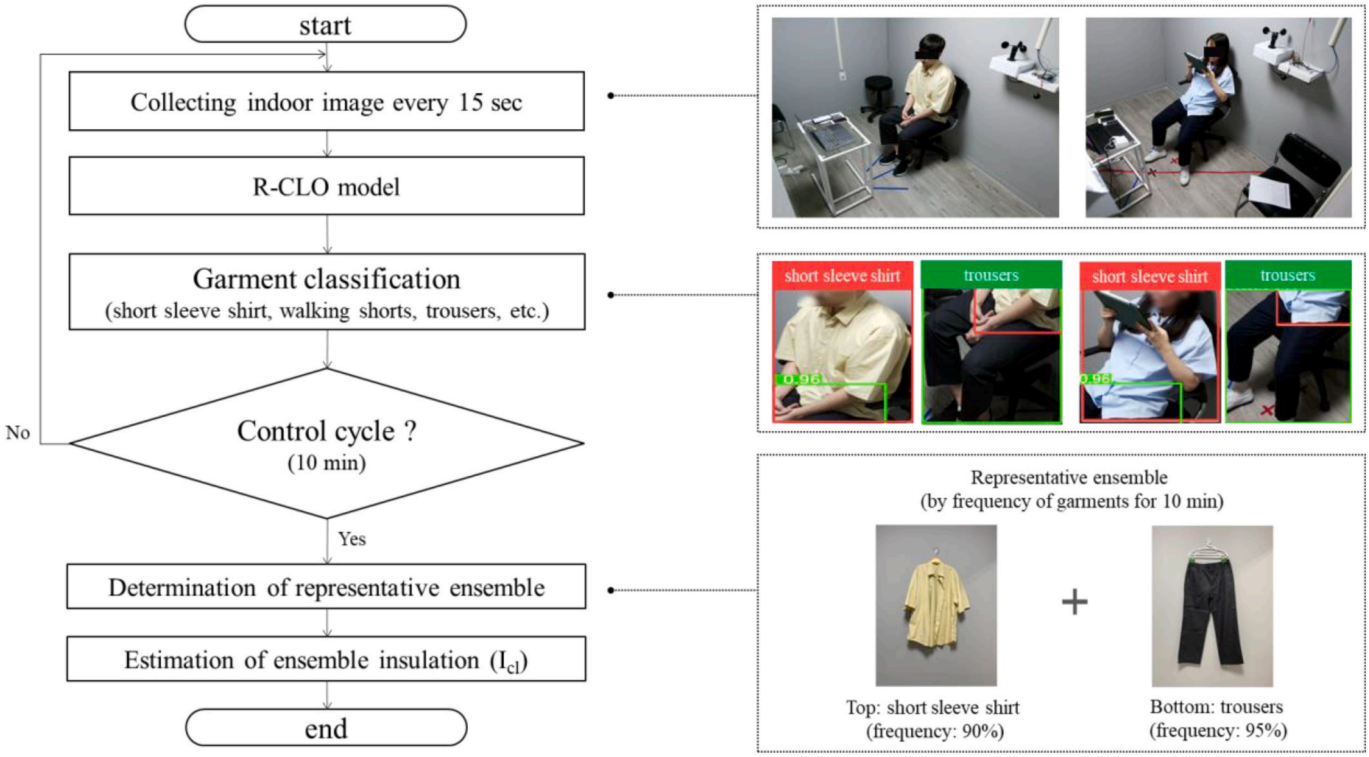

Fig. 2. I_{cl} decision algorithm employing the R-CLO model.

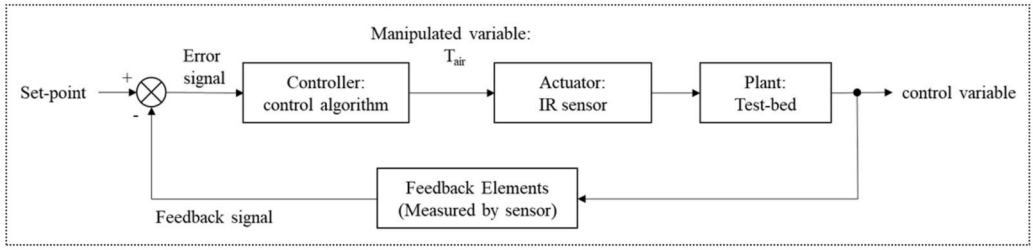

Control mode		Mode A	Mode B	Mode C (proposed method)
Control variable		T_a	PMV	PMV
Set-point		25 °C	0.0 (neutral)	0.0 (neutral)
Feedback elements	T_a	○	○	○
	RH	X	○	○
	T_r	X	○	○
	V_a	X	○	○
	Metabolic rate	X	Fixed value: 1.0 met	Fixed value: 1.0 met
	Clothing insulation (I_{cl})	X	Fixed value: 0.5 clo	Dynamic value (R-CLO model)
Feedback signal		Measured T_a	Calculated PMV	Calculated PMV

Fig. 3. Summary of the feedback control system.

PMV closest to 0 to reduce the error for the next control cycle.

In Mode B, the PMV was calculated based on four environmental variables (air temperature (T_a), relative humidity (RH), mean radiant temperature (T_r), and air velocity (V_a)) measured using sensors and arbitrarily fixed personal factors. This method has been widely used in situations where it is difficult to measure personal factors for PMV-based control [26,50,51]. The personal factors were based on ASHRAE Standard 55 [12], with the metabolic rate based on sitting and reading (1.0 met), which are common indoor activities and the clothing insulation set to 0.5 clo based on summer clothing standards. Using these sensor-based environmental variables and arbitrary personal factors as feedback elements, Mode B transmitted the calculated PMV as a feedback signal.

In Mode C, the proposed R-CLO model was employed, with the R-CLO results incorporated into the feedback elements, from which the PMV was calculated. I_{cl} is calculated using the R-CLO model and the I_{cl} decision algorithm described in Section 2.1. Thus, Mode C calculated the PMV based on the I_{cl} estimated using images and the four environmental variables measured using a sensor and sent this as a feedback signal.

2.3. Experimental information

2.3.1. Test bed

For the experiment, a test bed representing a real indoor environment was constructed and divided into two rooms of the same size (2.7

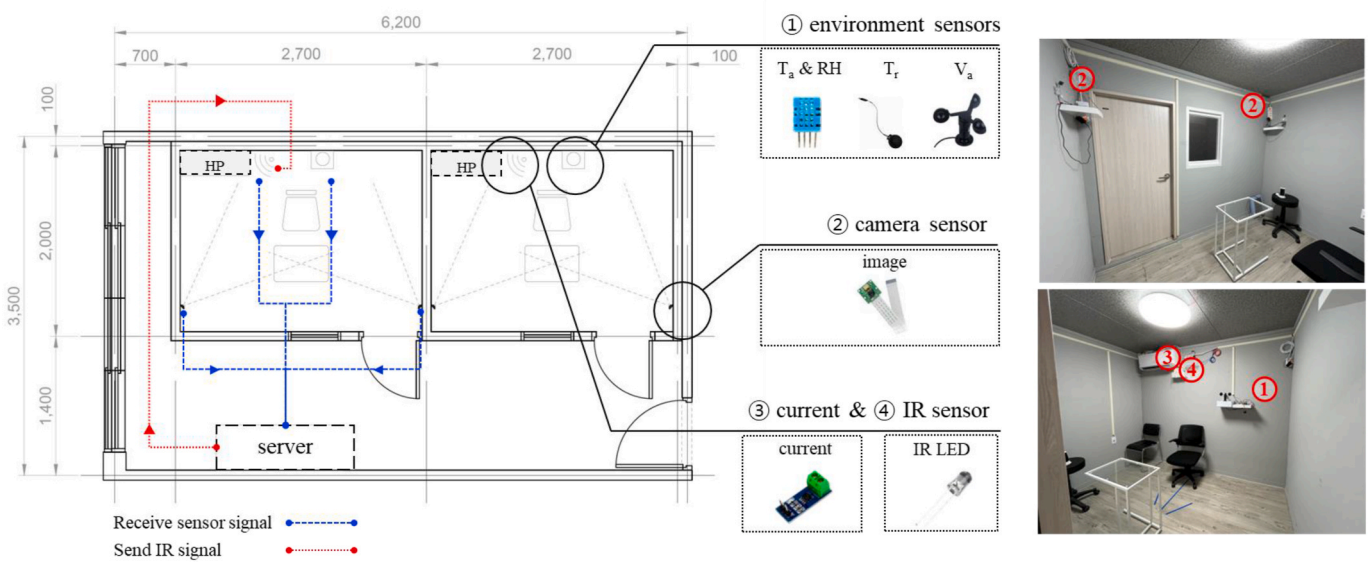

Fig. 4. Diagram of the sensors and signals employed in the test bed.

m × 2.0 m × 2.2 m). Each room had one window and one door, and the interior lighting used LED lamps. In addition, as a unitary air conditioning system, a packaged terminal heat pumps (PTHP) capable of heating and cooling was installed in each room to control the thermal environment. The coefficient of performance (COP) of the heat pump is 3.64 when operating in cooling mode, the cooling capacity was 2.8 kW. The power consumption was 770 W when the T_a is 27 °C DB/19 °C WB, and the outdoor air temperature is 35 °C DB/24 °C WB [52]. More detailed information about the system and the test bed is provided in Appendix A.

As shown in Fig. 4, the environment sensors were installed at a height of 1.2 m in the center of the wall to measure T_a, RH, T_r, and V_a. Camera sensors were installed at a height of 1.8 m on both sides of the room for image collection. An IR sensor for transmitting the set point temperature and a current sensor to output real-time electric power by measuring the current intensity were installed in connection with the air conditioning system. The installed sensors collected environmental data, images, and current data in real-time, which were transmitted using serial and TCP/IP communication to the server located in the hall outside the rooms. In the server, the PMV was estimated and the control signal determined using the collected data, and the control signal was transmitted to the IR sensor. The setting of the next control signal was repeated every control cycle. Because the metabolic rate of the occupants was fixed at 1.0 met, chairs and tables were provided to ensure the corresponding activity (e.g., sitting, writing, and/or reading) would occur. At this time, net chairs (0.00 clo) were used for this purpose to minimize their influence on the occupant's thermal sensation.

2.3.2. Data acquisition

The test bed had an integrated sensor module containing the environmental, camera, and current sensors for data collection and a server that processed data according to the control mode. The integrated sensor module was built based on Arduino and Raspberry Pi, which are single-board, open-source platforms. The platform is commonly used in home automation and security systems, is economical and highly scalable [53,54], and can effectively collect real-time data using TCP/IP and serial communication. In this experiment, the sensors measuring the environmental variables and current were configured to be Arduino-compatible, and a Raspberry Pi sensor was used for the camera.

The specifications of the integrated sensors installed in the test bed are presented in Table 2. The integrated sensor module collected information on four environmental variables (T_a, RH, T_r, and V_a), indoor images, and the electric energy consumption of the system. The entire sensors in the integrated sensor module was calibrated prior to the experiment to minimize measurement errors. In this experiment, the data collected every 15 s using the built-in integrated sensor module were stored on the server by Python. The images were input into the R-CLO model to estimate the real-time I_{cl}. The PMV was then calculated based on the I_{cl} and environmental data, and the optimal temperature to produce a PMV as close to 0 as possible was determined. The set temperature was transmitted to the air conditioning system via IR signal.

Table 2
Sensor specifications.

Parameter	Sensor	Specifications
Air temperature (T_a)	DHT 11	Range: 0–50 °C, Accuracy: ± 2 °C
Mean radiant temperature (T_r)	DHT 11	Range: 0–50 °C, Accuracy: ± 2 °C
Relative humidity (RH)	DHT 11	Range: 20–90%, Accuracy: ± 5%
Air velocity (V_a)	Three-cup anemometer	Range: 0–26.8 m/s Supply voltage: 4–10 V Measurement range: 0–30 m/s
Image	RPI 8 MP camera board	Resolution: 2592 × 1944 pixels, Transfer rate: 1080p−30 fps
Current	ACS712ELC-30A-T	TA (°C): −40 to 85 Optimized range, Ip (A): ±30 Sensitivity (mV/A): 66

2.3.3. Clothing ensemble schedule

In the experiment, nine clothing ensembles (E1−E9) that can be distinguished by the R-CLO model were investigated. These ensembles are presented in Table 3; they represent ensembles regularly worn in residential and office environments based on ISO 9920 [5] and ASHRAE Standard 55 [11]. One limitation of the R-CLO model is that it is difficult to classify clothing layers using images. This is difficult even for human classifiers without the active participation of the occupants, such as through surveys or the use of accurate measurement devices. Currently, the clothing layers are set arbitrarily according to the type of the outer garment detected, and the subjects were asked to wear the ensemble components equally.

I_{cl} was calculated using Eq. (1), which considered the I_{clu} for all of the individual garments worn by the subject, leading to an I_{cl} of between 0.38 and 1.04 clo for the ensembles (Table 3). For the experiment, all test subjects wore underwear (Males: briefs, 0.04 clo; Females: bra and panties, 0.04 clo), ankle socks (0.02 clo), and sneakers (0.02 clo). For E7−9, a sleeveless undershirt (0.06 clo) was added. The clothes were provided in men's and women's sizes using the same material wherever possible (see Table 1).

2.3.4. Experiment process

The experiment was conducted with one participant in each room, with each subject wearing an ensemble from Table 4 in random order. The experimental process presented in Fig. 5 was conducted for 40 min per ensemble. The system in the test bed controlled the indoor air temperature every 10 min via control signals received according to the control mode presented in Fig. 3. The first 10 min were set to allow the subjects to adapt to the room, and the experimental analysis was conducted over the remaining 30 min. Once the 40-min session had ended, a 15-min break was taken to allow the subjects to change their clothes. Consequently, the experiment was conducted for 210 min (40 min * 7 ensembles) for men and 360 min (40 min * 9 ensembles) for women for each control mode.

The subjects repeated the same experiment under Modes A, B, and C (see Fig. 3) and provided thermal sensation data for each environment. The experimental subjects participated over three days for Modes A, B, and C from September to early November, when the outside temperature was high. The subjective thermal sensation experienced by the subjects was measured using a seven-point TSV scale [12,31]. The survey was

Table 3
Summary of the clothing ensembles.

Ensemble	Clothing insulation (I_{cl})	Ensemble garments
E1	0.38 clo	Underwear, ankle socks, sneakers, T-shirt, walking shorts
E2	0.45 clo	Underwear, ankle socks, sneakers, short-sleeve shirtdress
E3	0.50 clo	Underwear, ankle socks, sneakers, short-sleeve shirt, walking shorts
E4	0.53 clo	Underwear, ankle socks, sneakers, short-sleeve shirt, knee-length skirt
E5	0.56 clo	Underwear, ankle socks, sneakers, short-sleeve pajama top, pajama trousers
E6	0.60 clo	Underwear, ankle socks, sneakers, long-sleeve sweatshirt, sweatpants
E7	0.66 clo	Underwear, ankle socks, sneakers, sleeveless undershirt, short-sleeve shirt, trousers
E8	0.74 clo	Underwear, ankle socks, sneakers, sleeveless undershirt, long-sleeve shirt, trousers
E9	1.04 clo	Underwear, ankle socks, sneakers, sleeveless undershirt, long-sleeve shirt, trousers, suit jacket

Table 4
Summary statistics for the participants in the experiment.

ID	Sex	Height (cm)	Weight (kg)	Age	BMI (kg/m^2)	Relative thermal sensation	Total number of surveys	Participation dates
1	Female	158	54	23	21.6	−1	503	9/23, 9/26, 10/14
2	Female	157	50	23	20.3	−1	565	9/27, 9/28, 10/5
3	Female	166	61	22	22.1	0	530	9/29, 10/2, 10/13
4	Male	178	67	24	21.1	0	440	9/30, 10/2, 10/3
5	Male	173	73	24	24.4	0	420	10/1, 10/8, 10/19
6	Male	177	70	29	22.3	0	419	10/5, 10/6, 10/13
7	Female	165	50	26	18.4	−1	531	10/7, 10/10, 10/31
8	Male	174	60	21	19.8	0	421	10/9, 10/17, 10/27
9	Female	157	52	22	21.1	0	556	10/9, 10/30, 10/31
10	Male	175	75	25	24.5	0	421	10/11, 10/23, 10/30
11	Female	160	49	35	19.1	−1	545	10/14, 10/20, 10/22
12	Female	165	54.5	24	20.0	−1	541	10/16, 10/17, 10/23
13	Female	157	46	24	18.7	−1	537	10/21, 10/25, 10/28
14	Male	176	74	25	23.9	0	421	10/20, 10/24, 10/27
15	Male	167	63	25	22.6	0	417	10/25, 10/29, 11/05

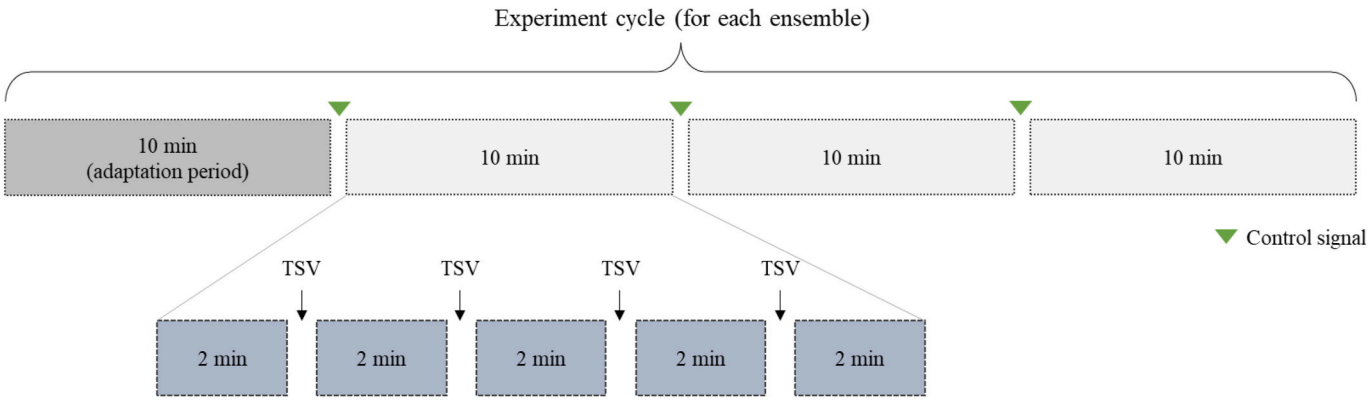

Fig. 5. Detailed experimental process for each ensemble.

conducted using 2-min cycles with point-in-time (right-now) surveys, with the items based on ASHRAE standard 55 [12], and the survey results were averaged over the control period. The surveys were conducted with cloud-based Google Forms. There were some missing data due to network disconnection problems or omitted responses by the subjects. Therefore, the total number of completed surveys differed slightly between the subjects. This information is specified in Table 4 of Section 2.3.5.

2.3.5. Subjects

The experimental subjects were 15 adults in their 20s and 30s. To minimize the effect of the body mass index (BMI) on the results, subjects with a normal BMI (18.5 kg/m^2 ≤ BMI <25 kg/m^2) were recruited. The summary statistics for the subjects are provided in Table 4. The mean BMI was 22.7 kg/m^2 (SD = 1.7 kg/m^2) for the men and 20.2 kg/m^2 (SD = 1.4 kg/m^2) for the women. The participation date in the experiment and the number of TSV survey data are also indicated.

Because there could be differences in the subjective thermal sensation for each subject, a preliminary experiment was employed, and the relative thermal sensation (TSVr) results presented in Table 4. This preliminary experiment was conducted in the same manner for all of the subjects, who reported their thermal sensation at a temperature of 25 °C and clothing insulation of 0.5 clo [11]. The test subjects wore the same short-sleeve shirt and walking shorts, and the TSVr was recorded as the most frequent TSV measured every minute over a 5-min period. All male subjects were identified as thermally neutral (i.e., TSVr = 0) under these conditions, while the female Subjects 1, 2, 7, 11, 12, and 13 felt slightly cold (i.e., TSVr = −1).

3. Results and discussion

3.1. Performance analysis for I_{cl} estimation

First, performance analysis for the R-CLO model was conducted for both the test dataset and in a real environment (Section 3.1.1), and then the performance of the I_{cl} decision algorithm with the actual subjects was conducted (Section 3.1.2). By evaluating the performance of the model in a real environment, this study intended to prove its accuracy and confirm its applicability to real buildings.

3.1.1. R-CLO model performance

When training the R-CLO model, the loss converged after around 80 epochs. The precision and recall for the training data were 0.94 and 0.92, respectively. The mAP (threshold = 0.5) for all of the classes was calculated to be 0.96, and the validation results for the optimal model with the lowest learning loss produced an object loss of 0.005, a bounding box loss of 0.011, and a classification loss of 0.008.

The performance results for the test dataset are presented in Figs. 6 and 7. Fig. 6 displays a confusion matrix for the classification performance of the model for the 16 garment classes. The X-axis represents the garments classified by the model, and the Y-axis represents the actual garments. The closer to 1.0 in the diagonal direction from the top left to the bottom right, the higher the accuracy. The average classification accuracy for all classes was 94.8%, and all garments except long-sleeve sweaters (88%) and long-sleeve shirtdresses (81%) had an accuracy of more than 90%. The main error for these two garments was that the long-sleeve sweater was misidentified as a long-sleeve sweatshirt, and the long-sleeve shirtdress was misidentified as a long-sleeve shirt or short-sleeve shirtdress.

Num	Garments	Num	Garments
1	short-sleeve shirt	9	walking shorts
2	long-sleeve shirt	10	sweatpants
3	T-shirt	11	suit jacket
4	long-sleeve sweater	12	long-sleeve shirtdress
5	long-sleeve sweatshirt	13	short-sleeve shirtdress
6	trousers (Straight, loose)	14	long-sleeve pajama top
7	knee-length skirt	15	long-sleeve pajama trousers
8	ankle-length skirt	16	short-sleeve pajama top

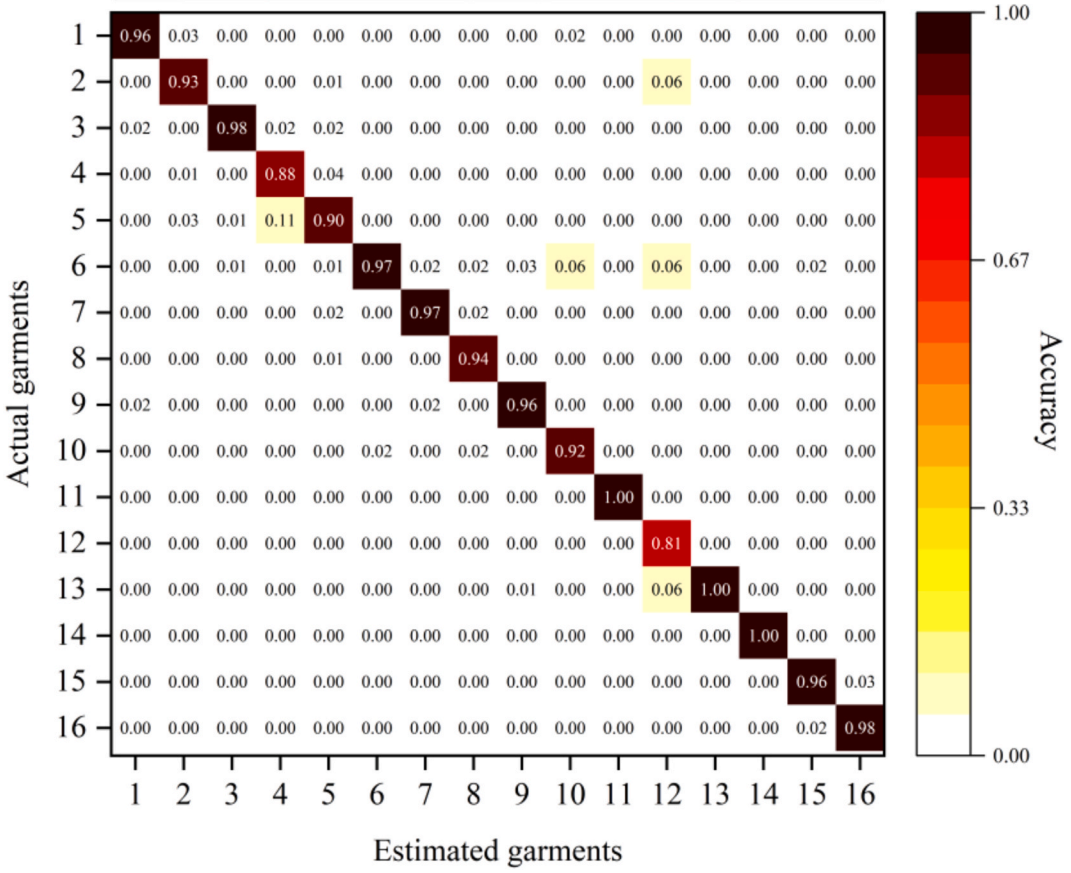

Fig. 6. Confusion matrix for the R-CLO model using the test dataset.

Fig. 7 presents examples from the R-CLO model for the detection and classification of clothes in the test dataset. The clothes in the image were able to be detected and classified from various angles. In addition, even if a body part, such as the upper body or face, was outside the image frame, it was possible to detect and classify the individual garments. In other words, the proposed model exhibited the potential to handle common situations that occur in a real environment, such as the collection of images from a variety of angles and certain areas not being captured by the images.

Although the accuracy of the test dataset averaged 94.7%, because the data were randomly extracted, the variance in the amount of data for each class was high, making it difficult to generalize the results under the same conditions. Therefore, additional experiments were conducted in an actual indoor environment to verify the performance of the model, and preliminary experiments were conducted for new spaces and participants that had not participated in the model training.

The participants in the preliminary experiment consisted of five researchers who each wore the nine different ensembles (E1−E9) and maintained a seated position in the test bed for 10 min each. Images were collected every 10 s from both angles in the laboratory, and a total of 5400 images (120 images per ensemble × 9 ensembles × 5 people) were used to evaluate the accuracy of the model and identify major errors.

Fig. 8 presents the experimental results for the 12 individual garments included in the nine ensembles. In the garment classifications, the short-sleeve shirtdress had an accuracy of up to 98.4%, and the top seven garments had an average accuracy of 88.4%. Commonly, errors occurred when a large area of the garments was covered due to the subject's posture or long hair or if the picture was out-of-focus due to movement by the subject. Because these errors can occur in real life when using images, this study attempted to resolve these issues by identifying the ensemble that occurred at the highest frequency for a specific period (see Section 2.1.3). For example, if there were two out-of-focus images due to the movement of the subject out of 80 images collected during a 10-min control cycle, this did not affect the determination of the representative ensemble. In other words, of the images acquired during a 10-min control cycle, transient and infrequent errors were treated as outliers and ignored when determining the representative ensemble for that control cycle.

The other five garments—long-sleeve sweatshirt, knee-length skirt, long-sleeve pajama trousers and top, and sweatpants—had a classification accuracy ranging from 10.6 to 43.4%. The main sources of error for these garments are presented in Fig. 8. Notably, most of the errors were caused by misclassifying them as garments with similar insulating areas. For example, long-sleeve pajama trousers and sweatpants were often classified as regular trousers, while short-sleeve pajama tops were

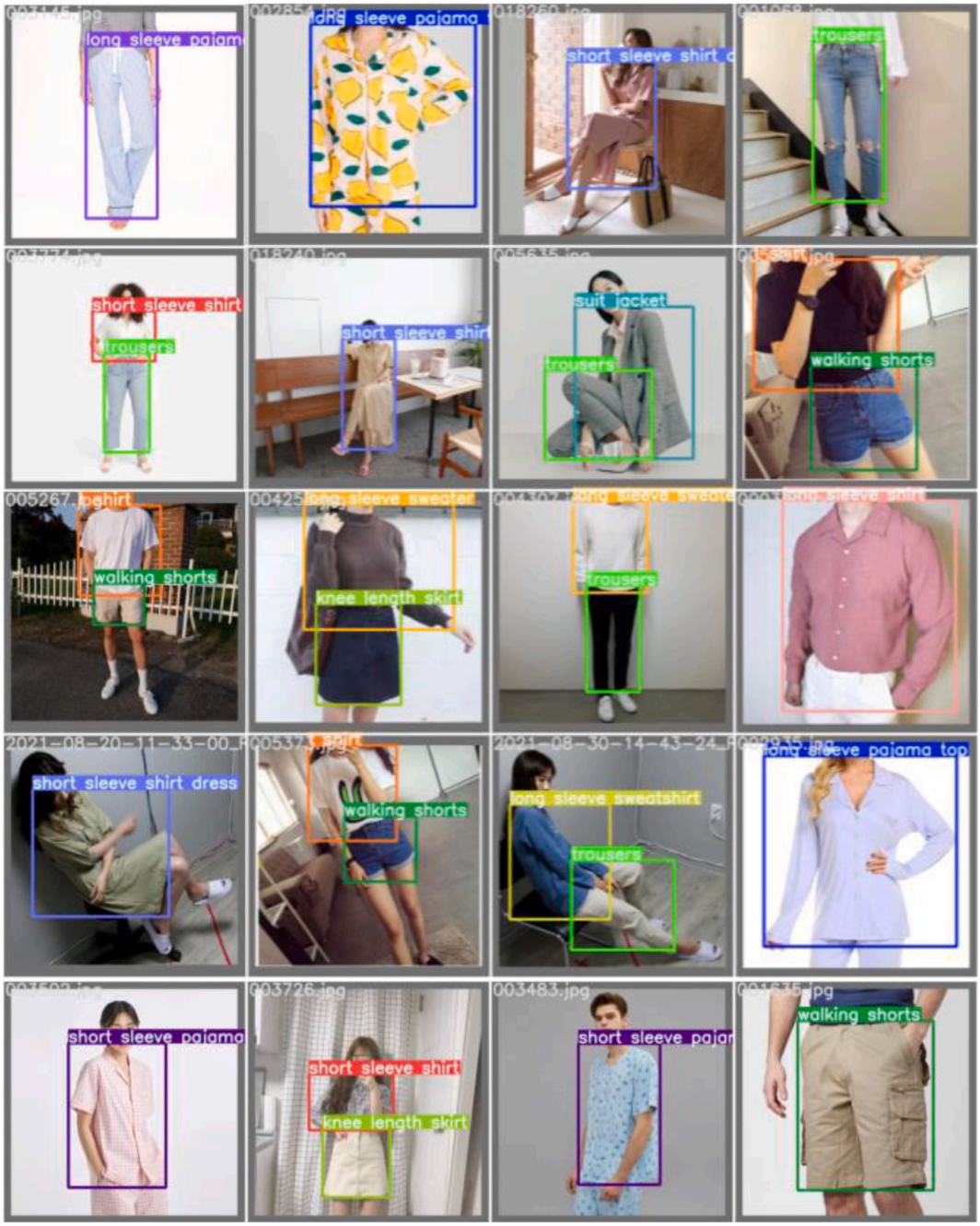

Fig. 7. Examples of R-CLO model results (test dataset).

mainly classified as short-sleeve shirts. In addition, because knee-length skirts were often worn together with a short-sleeve shirt, 68.9% of these skirts were misidentified as short-sleeve shirtdresses because the top and bottom garments were mistaken as a pair. However, because the insulating area of the garments was similar, the error in terms of I_{cl} was likely to be low.

3.1.2. *Accuracy analysis for representative I_{cl} estimation*

To control an indoor environment using the PMV, the I_{cl} for the ensembles worn by occupants during the control period is required. Therefore, an experiment was conducted using an I_{cl} decision algorithm (Section 2.1.3) that incorporated the proposed R-CLO model, and the accuracy of I_{cl} for a control cycle of 10 min was analyzed. The experiment was conducted with the subjects randomly wearing every ensemble, producing 405 I_{cl} datapoints. The accuracy of the I_{cl} for all of the subjects and the correct example from the I_{cl} decision algorithm for each ensemble is presented in Fig. 9 (a)–(b).

The dotted line in Fig. 9 (a) represents the actual I_{cl} of the ensembles (Table 3), and the solid line refers to the average value of the representative I_{cl} output from the algorithm. The table in the graph shows the error between the actual and estimated values. The average error of the model for all of the ensembles was 0.03 clo, and the maximum error was 0.06 clo. Except for E4 and E5, the ensembles had an error of less than 0.03 clo. The pants in E5 and E6 (pajama trousers and sweatpants, respectively) were often classified as trousers, the same error as seen in Fig. 8. Therefore, errors also occurred in the representative I_{cl} values. However, even if an error occurred, the average I_{cl} error was not as large as ±0.03 clo. As an example, an I_{cl} error of ±0.03 clo would lead to variation in the PMV of ±0.06 under the environmental conditions set for Mode A ($T_a = 25.3\ ^\circ C$; RH = 62.7%; $T_r = 24.7\ ^\circ C$; $V_a = 0.0$ m/s) with

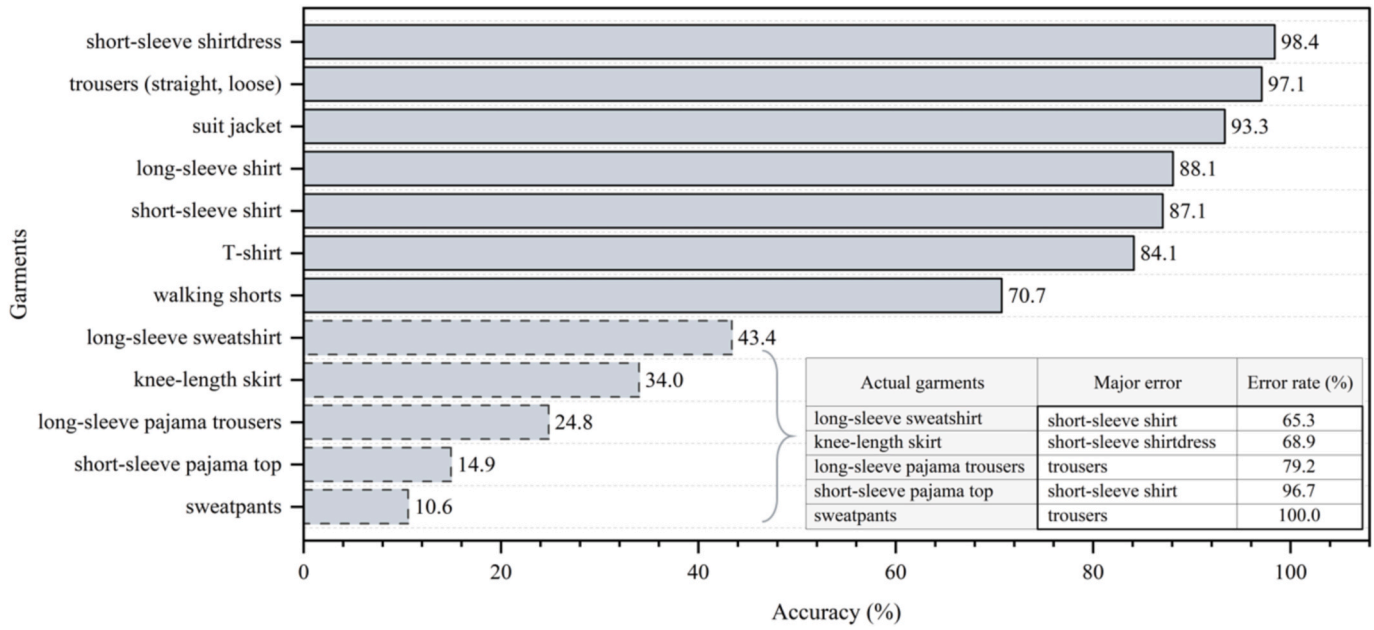

Fig. 8. Accuracy of garment classification using the R-CLO model in a real environment.

subject ID 8. Many of the misidentifications had a similar insulation area as the actual garment. The error for E4 (knee-length skirt and short-sleeve shirt) averaged 0.06 clo, which was mainly due to misidentification as a short-sleeve shirtdress with a similar coverage area for the human body.

I_{cl} errors caused by poses or long hair obscuring parts of the body and out-of-focus images were mostly treated as outliers, thus the representative I_{cl} was unaffected. In addition, even though some errors occurred in estimating I_{cl}, it was necessary to analyze the effect of Mode C, which reflects real-time clothing insulation, on thermal comfort and electrical energy consumption compared with conventional control methods.

To confirm the suitability of the proposed method for estimating real-time I_{cl}, its results were compared with previous studies that developed image-based models to estimate clothing insulation. In previous research, models that classify only individual garments [27,38] and that classify ensembles [40,42] have been developed. In particular, Liu et al. [27] developed a model that classified five types of top garment according to the area of the upper body, and the classification accuracy was high at 95.17%. Miura et al. [38] estimated I_{clu} using three types of top garment, and the maximum error was reported to be −0.95 clo. On the other hand, a model that classified the entire clothing ensemble rather than individual garments was developed to classify five ensembles, producing an accuracy of 86% in a real environment [40].

The R-CLO model proposed in the present study estimates the I_{cl} of ensembles based on the garment classification. It thus has the advantage of considering individual garments and clothing ensembles simultaneously. The garment classification performance of the developed model exhibited an average accuracy of 94.8% for the test dataset. This is notable because 16 types of garment were classified, more than twice as many as in previous models. In addition, the number of ensembles that could be identified based on this 16-garment classification system was at least 34. Thus, the R-CLO model can be considered to be more applicable to real environments. It was also shown that I_{cl} can be estimated with an average error of 0.03 clo using nine representative ensembles. Thus, the proposed model offers improved performance and greater applicability compared to previously reported models.

3.2. Analysis of the experimental results

3.2.1. Environmental factors

In this section, the thermal environment was evaluated based on data collected from the experiment testing the three control modes (see Fig. 3). Experimental data were collected at 15-s intervals and corrected with average data in 2-min units, generating 5370 experimental datapoints for analysis. Each datapoint included the four indoor environmental variables (Ta, RH, Tr, and Va), clothing insulation information, the PMV, and the TSV for the test subject. Prior to analysis, outliers caused by system operation errors such as sensor errors and network disconnection during data collection were removed. The thermal environment was analyzed in terms of the operative temperature (T_o). Across all subjects during the experiment, the indoor relative humidity had a range of around 30–70%, and V_a averaged 0.08 m/s or lower.

The change in T_o for each control mode depending on the clothing ensemble is presented in Fig. 10. Because the set point for the indoor air temperature differed between the three modes, the indoor T_o also differed. Mode A set the temperature at 25 °C, thus T_o was maintained at an average of 24.5 °C. Mode B employed PMV-based control with fixed values for personal factors, including I_{cl} (0.50 clo), while the environmental variables varied according to the sensor measurements. As a result, for all control points during the experiment, the indoor set temperature was 26 °C, and the indoor average T_o was 25.1 °C, about 0.6 °C higher than for Mode A.

In Mode C, I_{cl} differed from E1 (0.38 clo) to E9 (1.04 clo), thus the set temperature for each control point was 23–27 °C. The average T_o was highest at 25.6 °C for E1 and the lowest at 23.3 °C for E9. In Modes A and B, the indoor T_o was constant irrespective of the clothing, whereas, in Mode C, the temperature varied dynamically according to the clothing.

3.2.2. Thermal comfort

The actual PMV distribution for the subjects in the created indoor environment is displayed in Fig. 11. Fig. 11 (a)–(c) shows the average and 99% confidence intervals (CIs) for the PMV derived from the synthesis of the results calculated at 2-min intervals for Modes A, B, and C. The average PMV difference between E1 (0.38 clo) and E9 (1.04 clo), which had the largest difference in I_{cl}, was highest for Mode A (1.3), followed by Mode B (1.2) and Mode C (0.5). The difference in the average PMV for Modes A and B was thus twice as high as that for Mode

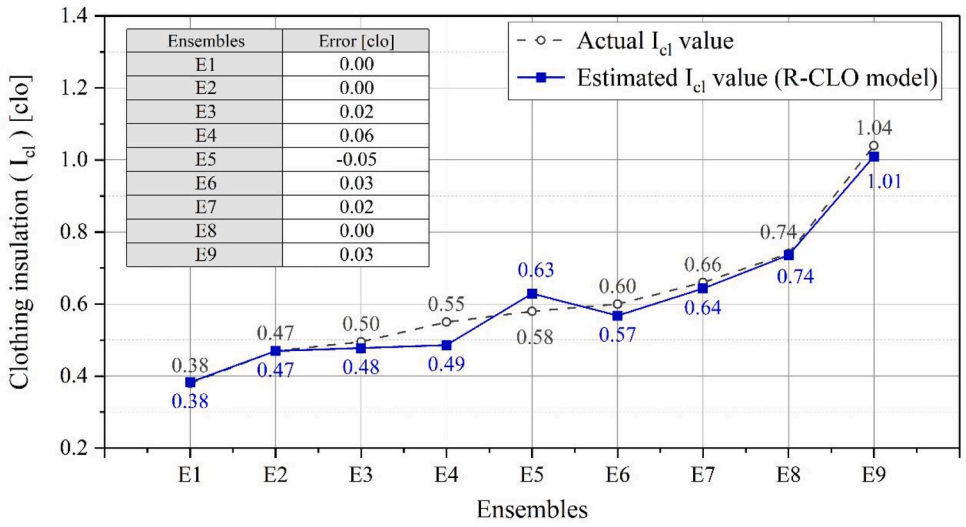

a)

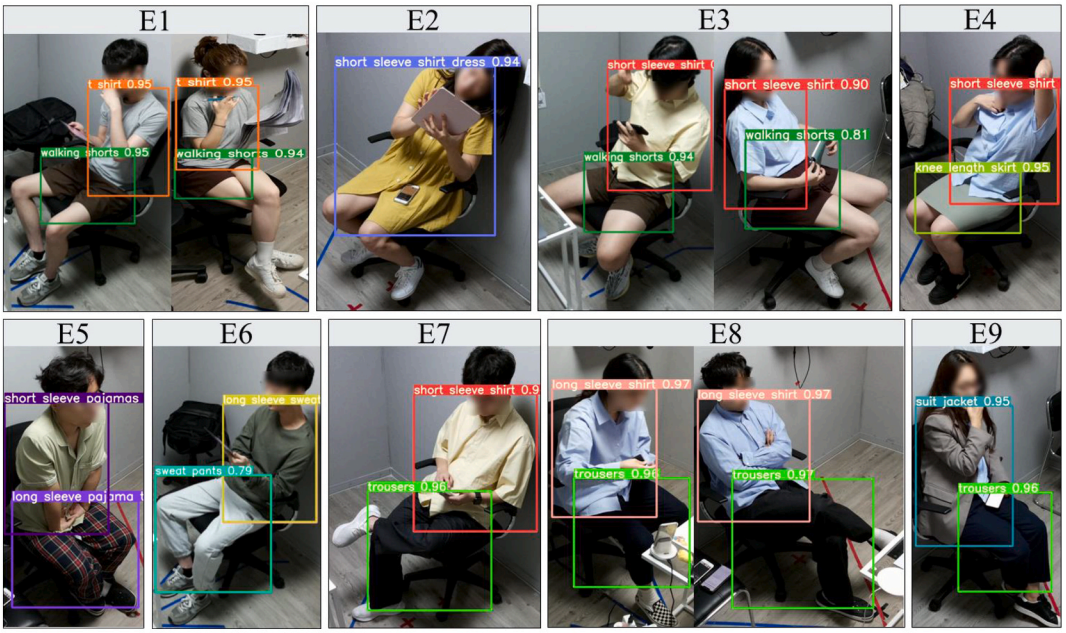

b)

Fig. 9. Experimental results for the R-CLO model: a) estimation accuracy of the clothing insulation using the proposed model and b) output examples of the correct results.

C, with the PMV increasing as I_{cl} increased. On the other hand, the average PMV for Mode C ranged between −0.51 and 0.08 depending on the clothing ensemble, confirming that the occupants had the highest thermal comfort when this mode was employed.

In Mode A, the PMV was lower than the other modes for E1−E3 because it generated the lowest temperature (Fig. 10). In particular, there was a large difference in the PMV for E1 and E9 according to the control mode. For E1, the average PMV for Modes A, B, and C were −0.86, −0.67, and −0.51, respectively, with Mode C closest to the comfort range. In Mode C, 53.3% of the datapoints satisfied the comfort range, which was higher than that for Modes A and B (16.7% and 20.0%, respectively).

The average PMV was 0.2 in E9 using Mode C, which was close to a neutral state. For E9, 60.0% and 53.3% of the datapoints were outside the comfort range for Modes A and B, respectively, while Mode C satisfied the comfort range for all datapoints. For E4 (0.55 clo) to E8 (0.74 clo), the average PMV was between −0.50 and 0.50 for all three control modes, with E2 (0.47 clo) and E3 (0.50 clo) fully falling within the comfort range, except with Mode A.

In summary, the control method with the highest comfort satisfaction was Mode C, while the lowest was Mode A. Additionally, all three control methods satisfied the comfort range for E4−E8, but Mode C had the highest satisfaction rate for ensembles with a large difference from 0.5 clo. Therefore, PMV control that considers real-time I_{cl} is more advantageous than other control methods under various clothing conditions.

The TSV results for the thermal comfort of the actual subjects are displayed in Fig. 12. The TSV was investigated every 2 min. The vertical

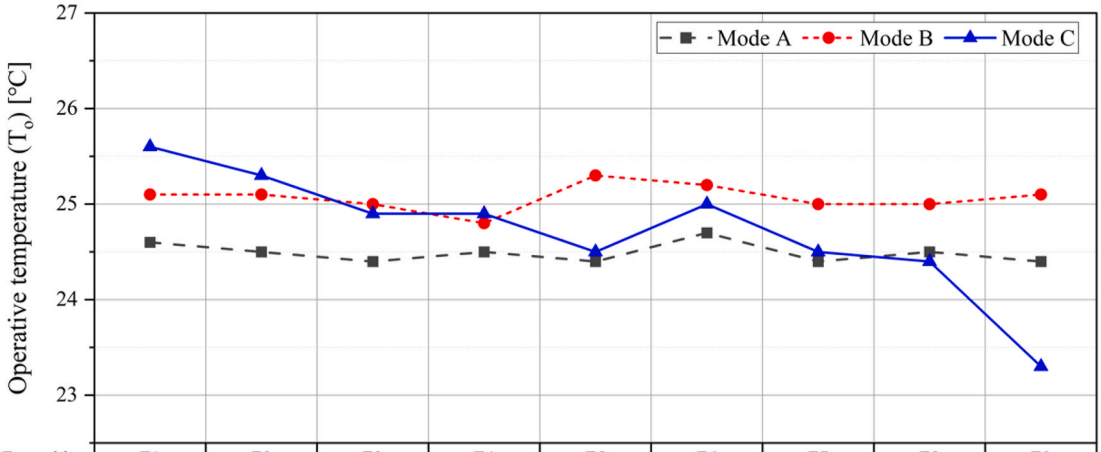

Ensembles	E1	E2	E3	E4	E5	E6	E7	E8	E9
Mode A	24.6	24.5	24.4	24.5	24.4	24.7	24.4	24.5	24.4
Mode B	25.1	25.1	25.0	24.8	25.3	25.2	25.0	25.0	25.1
Mode C	25.6	25.3	24.9	24.9	24.5	25.0	24.5	24.4	23.3

Fig. 10. Average indoor operative temperature (T_o) according to the control mode.

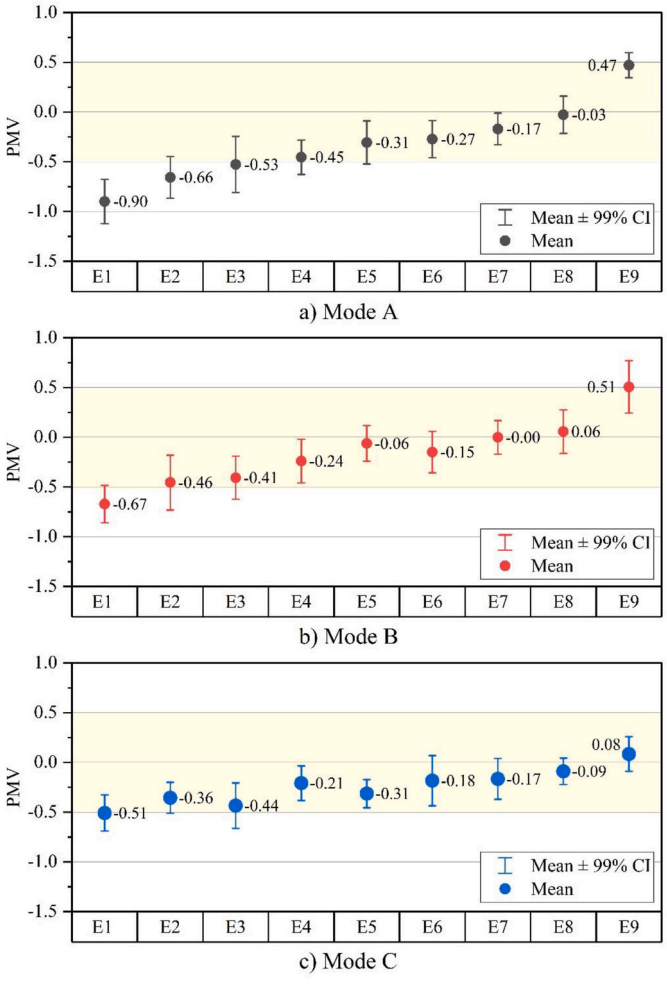

Fig. 11. Distribution results for the calculated PMV: a) Mode A, b) Mode B and c) Mode C.

endpoint of the diamond plots in the figure indicates that 50% of the data falls within 25–75%, and the asterisk denotes the average value. The area corresponding to the comfortable range is indicated in yellow.

The average TSV results differed slightly from the PMV results. In Mode A, the average TSV for E1, E2, and E4, which had a low I_{cl}, were −0.61, −0.92, and −0.73, respectively. This means that the subjects felt slightly cool in Mode A. Except for these ensembles, the average TSV was between −0.5 and 0.5, indicating a comfortable state. The average TSV for Modes B and C exhibited similar results, with a difference of up to 0.28, and the comfort range was satisfied for all ensembles. Of the three modes, Mode A produced the highest percentage (38%) of datapoints outside the comfort range, while Modes B and C had similar percentages (20% and 24%, respectively). Most of the datapoints outside the comfort range were within the range of $-2.0 < TSV < -0.5$.

The TSV measures subjective thermal sensation, and these results could be related to the TSVr summarized in Table 4. Six subjects had a TSVr of −1 (Subjects 1, 2, 7, 11, 12, and 13), and the discomfort rate may have been higher for these subjects. The proportion of datapoints from subjects with TSVr = −1 within the discomfort range ($-2.0 < TSV \leq -0.5$) was 60% and 40% for Modes A and B, respectively, compared to around 85% for Mode C. Thus, the indoor air temperature set using Mode C could cause discomfort by creating a rather cold environment for occupants with a low TSVr, especially for E7−9.

3.2.3. *Analysis of electrical energy*

In the thermal comfort analysis, it was confirmed that Mode C was the most advantageous control method in terms of the PMV. Based on these results, the electrical energy of the air conditioning system was analyzed in terms of electric power consumption by control mode in cooling mode. Fig. 13 presents the average electrical energy for each ensemble used during the experiment accumulated for a total of 181.5 h (10.5 h each for seven men, 13.5 h each for eight women) for all subjects.

There was no significant difference in electrical energy between the ensembles for either Mode A or B. The average electrical energy used for all ensembles was 140 Wh and 103 Wh for Modes A and Mode B, respectively, primarily due to a 1 °C set point temperature difference between the two modes. On the other hand, for Mode C, the indoor air temperature was set to be lower as I_{cl} increased. Accordingly, the electrical energy tended to increase as I_{cl} increased, and the average electrical energy for E9 was more than 2.2 times higher than for E1.

The total consumption for Modes A, B, and C were 19.8 kWh, 14.9 kWh, and 17.3 kWh, respectively. Mode C used 12.6% less energy compared with Mode A but used 16.1% more than Mode B. The total electrical energy in this experiment was the result of wearing each

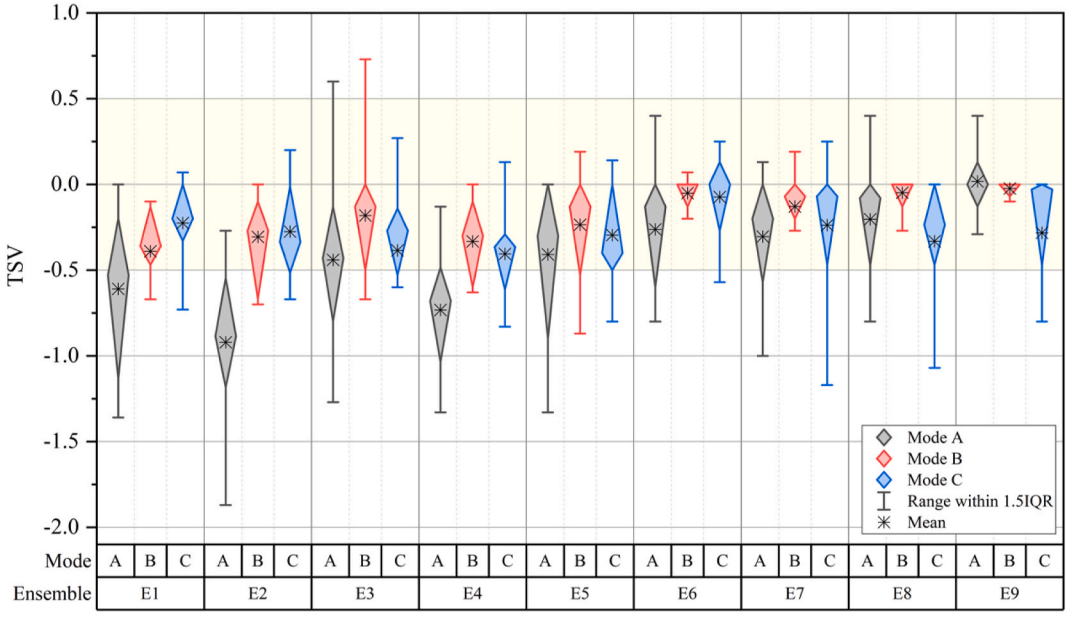

Fig. 12. Average TSV distribution according to the control mode.

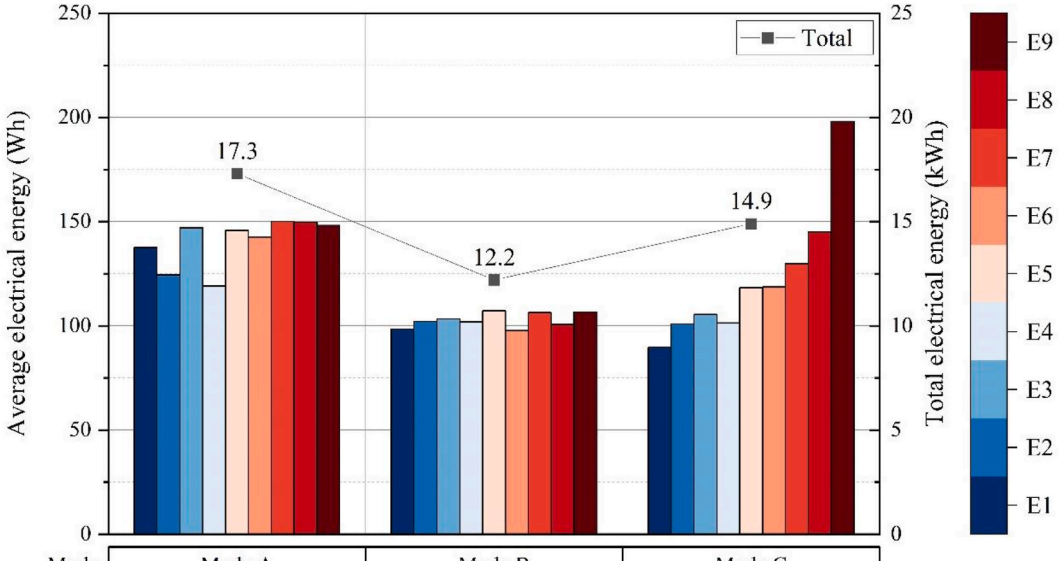

Mode	Mode A	Mode B	Mode C
E1	137.6 Wh	98.4 Wh	89.7 Wh
E2	124.4 Wh	102.1 Wh	100.9 Wh
E3	147 Wh	103.2 Wh	105.5 Wh
E4	119.1 Wh	101.9 Wh	101.4 Wh
E5	145.8 Wh	107.2 Wh	118.3 Wh
E6	142.5 Wh	97.7 Wh	118.7 Wh
E7	150.1 Wh	106.3 Wh	129.8 Wh
E8	149.7 Wh	100.6 Wh	145 Wh
E9	148.1 Wh	106.6 Wh	198 Wh

Fig. 13. Electrical energy according to ensemble and control mode.

ensemble for the same 30 min, however, it can vary depending on the clothes that are worn in an actual building. For example, Mode C set the T_a to 26–28 °C for E1, which decreased the electric energy consumption by 34.8% and 8.8%, compared to Modes A and B, respectively. Conversely, for E9, Mode C required 33.7% and 85.7% more electric energy than Modes A and B, respectively, because the indoor air temperature was set to 23–24 °C, which was lower than the other modes.

Fig. 14 presents the electrical energy use of E1 and E9, which had the

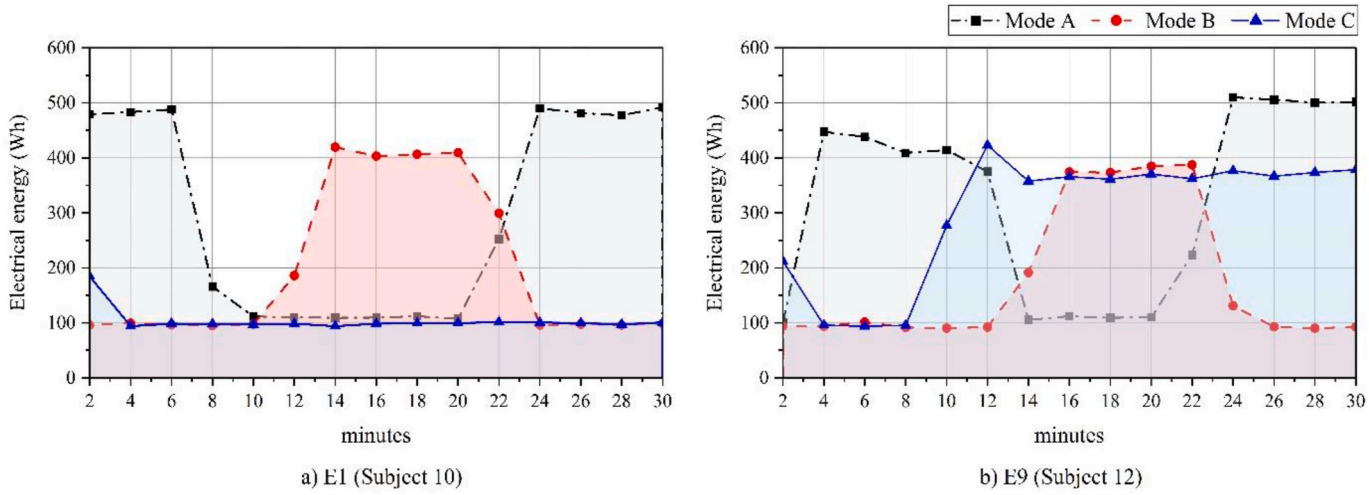

Fig. 14. Variation of the electrical energy use over time by control mode: a) E1 (Subject 10) and b) E9 (Subject 12).

largest difference in clothing insulation, for each mode over time. For E1, Mode C set a higher indoor air temperature, thus the cooling system was rarely employed and only standby power was used (Fig. 14a). On the other hand, for E9 in Fig. 14 (b), because Mode C set the lowest indoor air temperature, the system was operated in most time, and more electrical energy was used than with the other control modes. In other words, Modes A and B managed the system in a constant manner regardless of I_{cl}, whereas, in Mode C, the operating time and electrical energy of the system varied depending on I_{cl}.

In summary, this section highlighted that the electrical energy can be differed depending on the type of clothing for proposed control Mode C. If the clothing occupants wear can be considered in real-time, the indoor environment can be controlled in a way that minimizes the energy at a suitable comfort level in an actual building. Therefore, real-time I_{cl} must be accurately reflected in an optimal control system that considers both comfort and energy consumption in an actual building.

4. Conclusions

This study sought to control the indoor environment using the PMV as a control variable based on I_{cl} information in real-time and to confirm its effect on thermal comfort and energy use. A CNN-based image processing R-CLO model was developed to estimate real-time I_{cl}, and a PMV-based control method reflecting the R-CLO model was designed. Using the developed model and control method, a thermal environment control experiment was conducted on subjects in a real environment. The performance of the proposed PMV-based control method with real-time I_{cl} (Mode C) was compared with existing thermal environment control methods (DBT-based control and PMV-based control with fixed I_{cl}; Modes A and B, respectively). The main results of this study are summarized below.

1. The R-CLO model was able to classify 16 individual garments using RGB images and estimate the I_{cl} for more than 34 clothing ensembles. The R-CLO model had an average accuracy of 94.7% for all garments based on the test dataset, while the I_{cl} estimation error in a real environment was found to be as low as 0.03 clo on average. In addition, it was confirmed that the errors caused by clothing occlusion and out-of-focus images can be treated as outliers by employing an I_{cl} decision algorithm.
2. In the thermal environment control experiment for the three control modes, Modes A and B employed a fixed set point temperature regardless of changes in clothing, while Mode C adjusted the indoor set point temperature according to changes in clothing. As a result of the PMV analysis, Mode C outperformed the other modes in terms of maintaining the PMV within the comfort range for all clothing conditions. In addition, actual TSV surveys of the subjects confirmed that, unlike Mode A, the average TSV for Modes B and C was between −0.5 and 0.5 for all ensembles, representing a comfortable state.
3. In terms of electrical energy, there was no significant difference in the electrical energy consumption in cooling mode for Modes A and B with changes in I_{cl}. On the other hand, because Mode C controls the indoor air temperature considering I_{cl}, the electric energy increased in proportion to I_{cl}. For example, E9 led to the use of 2.2 times more energy than did E1. This shows that the most advantageous control method in terms of electrical energy use in an actual building environment can vary depending on the type of clothing that the occupants wear. The need for real-time information on I_{cl} was confirmed for optimal operation to reduce building energy use.

The results of this study contribute to building management and control by suggesting a technology for estimating I_{cl} in real-time so that it is possible to manage a building environment in a way that considers both thermal comfort and energy consumption. However, this study performed thermal comfort analysis for single occupants at a time; additional research should be conducted to detect individuals and their I_{cl} for multiple occupants at the same time. In addition, since PMV is affected by altitude, further research should be conducted on occupants living in high-altitude areas such as La Paz in Bolivia, or even the passengers inside an airplane [55,56]. Moreover, because the proposed method may not satisfy the comfort range depending on the relative thermal sensation of the occupants, additional efforts are needed to increase the satisfaction rate for thermal comfort by providing a customized environment for the occupants through model adaptive learning based on the TSV.

As mentioned above, it was difficult to distinguish the clothing layers using the image processing model. Currently, all of the layers except for outerwear are set arbitrarily. Thus, additional research is needed to accurately estimate clothing insulation through layer classification. Additionally, the types of clothing that can be classified will be expanded so that the model can be applied to actual built environments.

Additional experiment will be conducted on the heating period and perform a comparative analysis with the results of this study. It is also necessary to confirm the changes in thermal comfort and energy consumption associated with the PMV in a way that also considers the metabolic rate. In addition, if an HVAC system with a finer temperature resolution is used, more accurate comfort control will be possible [31]. Additional energy consumption analysis is thus required for various HVAC system types and capacities.

CRediT authorship contribution statement

Eun Ji Choi: Writing – review & editing, Writing – original draft, Visualization, Validation, Supervision, Software, Methodology, Formal analysis, Data curation. **Bo Rang Park:** Writing – original draft, Validation, Resources, Investigation, Data curation. **Nam Hyeon Kim:** Visualization, Resources, Formal analysis, Data curation. **Jin Woo Moon:** Writing – review & editing, Supervision, Project administration, Methodology, Funding acquisition, Formal analysis, Conceptualization.

Declaration of competing interest

The authors declare that they have no known competing financial interests or personal relationships that could have appeared to influence the work reported in this paper.

Data availability

The authors do not have permission to share data.

Acknowledgments

This work was supported by the National Research Foundation of Korea (NRF) grant funded by the Korean government (MSIT) (2019R1A2C1084145) and by the Korea Institute of Energy Technology Evaluation and Planning (KETEP) and the Ministry of Trade, Industry and Energy (MOTIE) of the Republic of Korea (No. 20212020800120).

Appendix A. Configuration of the test bed

A1. Test bed configuration

The test bed is inside the building, and every side of the test bed except the rear of the room are in contact with the indoor space as presented in Fig. A1. It consisted of two rooms with the same structure. Details of the envelope elements such as size and U-value, and installed systems are shown in Table A1. In the test bed, an inverter type of packaged terminal heat pumps (PTHP) is installed for indoor air conditioning. In addition, the room is naturally ventilated, and no additional ventilation system was installed.

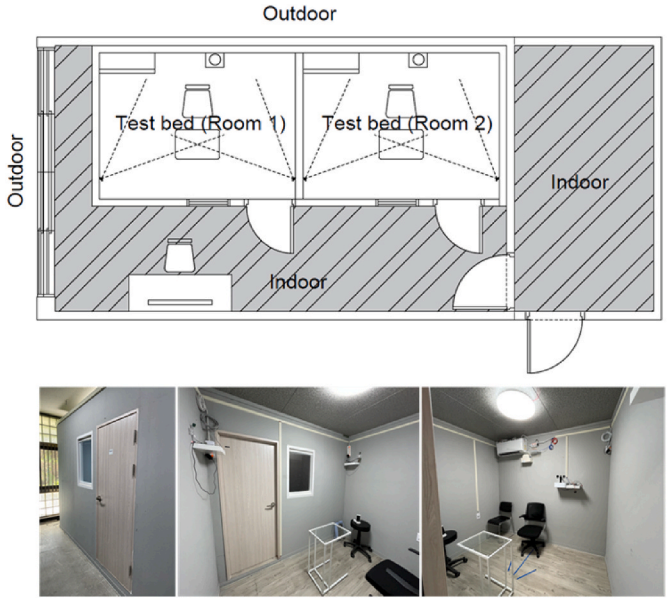

Fig. A1. Test bed plan

Table A1
Structural properties of the test bed

Test bed configuration		Information
Envelopment	Floor area (m)	2.68 × 2.00
	Height (m)	2.2
	Door (W × H × D) mm	800 × 1800 × 30
	Window (W × H) mm	600 × 800
	U-value (W/m^2k)	wall & roof: 0.33
		floor: 1.35
Air conditioning system		Inverter type of packaged terminal heat pumps (PTHP)
Ventilation system		natural ventilation (window closed)

A2. Specification of the installed air conditioning system

The air conditioning system installed for the experiment is an inverter-type PTHP unit commonly used at home that can use electricity as a fuel for heating and cooling. The major variables that affect electrical energy, such as system capacity, COP and power consumption, are detailed in Table A2. The power consumption was 770 W in cooling mode when the Ta is 27 °C DB/19 °C WB, and the outdoor air temperature is 35 °C DB/24 °C WB [52]. The system performs on/off control based on setpoint temperature and has deadband of 2 °C.

In the experiment, the room air temperature was controlled according to the set temperature signal, and the fan speed was fixed to low mode. The electrical energy of the system was calculated based on the voltage output through the current sensor (described in Table 2) that measures the AC/DC currents as analog values.

Table A2
Air conditioning system specification

System specification		PTHP
Model		Carrier CSV-Q075BI
Total air-conditioned floor area (m^2)		22.8
Capacity	Cooling capacity (kW)	rated: 2.80 (min:1.25/max: 3.20)
	Heating capacity (kW)	rated: 3.50 (min:1.20/max: 4.50)
COP	Cooling	3.64
	Heating	3.89
Power consumption	Cooling (kW)	0.77
	Heating (kW)	0.90
Power supply	Volt/Phase/Hz	220/1/60
Dimension	Indoor (W × H × D) mm	798 × 293 × 240
	Outdoor (W × H × D) mm	550 × 780 × 290
Weight	Indoor (kg)	9.0
	Outdoor (kg)	28.0
Refrigerant	Type	R410A
Control	Type	On/Off control

References

[1] K.W. Tham, H.C. Willem, Room air temperature affects occupants' physiology, perceptions and mental alertness, Build. Environ. 45 (1) (2010) 40–44.
[2] D.P. Wyon, The effects of indoor air quality on performance and productivity, Indoor Air 14 (2004) 92–101.
[3] W.J. Fisk, A.H. Rosenfeld, Estimates of improved productivity and health from better indoor environments, Indoor Air Int. J. Indoor Air Qual. Clim. 7 (3) (1997) 158–172.
[4] F. Zhang, R. de Dear, P. Hancock, Effects of moderate thermal environments on cognitive performance: a multidisciplinary review, Appl. Energy 236 (2019) 760–777.
[5] A. Wagner, E. Gossauer, C. Moosmann, T. Gropp, R. Leonhart, Thermal comfort and workplace occupant satisfaction - results of field studies in German low energy office buildings, Energy Build. 39 (7) (2007) 758–769.
[6] I. Kang, K.H. Lee, J.H. Lee, J.W. Moon, Artificial neural network-based control of a variable refrigerant flow system in the cooling season, Energies 11 (7) (2018).
[7] J.W. Moon, J. Ahn, Improving sustainability of ever-changing building spaces affected by users' fickle taste: a focus on human comfort and energy use, Energy Build. 208 (2020).
[8] J.W. Moon, J.C. Park, S. Kim, Development of control algorithms for optimal thermal environment of double skin envelope buildings in summer, Build. Environ. 144 (2018) 657–672.
[9] L.J. Wang, J. Kim, J. Xiong, H.G. Yin, Optimal clothing insulation in naturally ventilated buildings, Build. Environ. 154 (2019) 200–210.
[10] P.O. Fanger, Thermal Comfort. Analysis and Applications in Environmental Engineering, Danish Technical Press, Copenhagen, 1970.
[11] ISO 7730:2005, Ergonomics of the Thermal Environment — Analytical Determination and Interpretation of Thermal Comfort Using Calculation of the PMV and PPD Indices and Local Thermal Comfort Criteria, European Committee for Standardization, UK, 2005.
[12] ASHRAE Standard 55, Thermal Environmental Conditions for Human Occupancy, American Society of Heating, Refrigerating and Air-Conditioning Engineers, Atlanta, GA, USA, 2017.
[13] CEN 15251, Indoor Environmental Input Parameters for Design and Assessment of Energy Performance of Buildings: Addressing Indoor Air Quality, Thermal Environment, Lighting and Acoustics, European Committee for Standardization, Brussels, 2007.
[14] W. O'Brien, A. Wagner, M. Schweiker, A. Mahdavi, J. Day, M.B. Kjaergaard, S. Carlucci, B. Dong, F. Tahmasebi, D. Yan, T.Z. Hong, H.B. Gunay, Z. Nagy, C. Miller, C. Berger, Introducing IEA EBC annex 79: key challenges and opportunities in the field of occupant -centric building design and operation, Build. Environ. 178 (2020).
[15] F. Jazizadeh, A. Ghahramani, B. Becerik-Gerber, T. Kichkaylo, M. Orosz, Human-building interaction framework for personalized thermal comfort-driven systems in office buildings, J. Comput. Civ. Eng. 28 (1) (2014) 2–16.
[16] J. Kim, S. Schiavon, G. Brager, Personal comfort models - a new paradigm in thermal comfort for occupant-centric environmental control, Build. Environ. 132 (2018) 114–124.
[17] J.Q. Xie, H.Y. Li, C.T. Li, J.S. Zhang, M.H. Luo, Review on occupant-centric thermal comfort sensing, predicting, and controlling, Energy Build. 226 (2020).
[18] M. Zang, Z.Q. Xing, Y.Q. Tan, IoT-based personal thermal comfort control for livable environment, Int. J. Distributed Sens. Netw. 15 (7) (2019).
[19] D. Li, C.C. Menassa, V.R. Kamat, Robust non-intrusive interpretation of occupant thermal comfort in built environments with low-cost networked thermal cameras, Appl. Energy 251 (2019).
[20] A. Ghahramani, G. Castro, S.A. Karvigh, B. Becerik-Gerber, Towards unsupervised learning of thermal comfort using infrared thermography, Appl. Energy 211 (2018) 41–49.
[21] S.C. Liu, S. Schiavon, H.P. Das, M. Jin, C.J. Spanos, Personal thermal comfort models with wearable sensors, Build. Environ. 162 (2019).
[22] S. Carlucci, M. De Simone, S.K. Firth, M.B. Kjaergaard, R. Markovic, M.S. Rahaman, M.K. Annaqeeb, S. Biandrate, A. Das, J.W. Dziedzic, G. Fajilla, M. Favero, M. Ferrando, J. Hahn, M. Han, Y. Peng, F. Salim, A. Schluter, C. van Treeck, Modeling occupant behavior in buildings, Build. Environ. 174 (2020).
[23] S. Kim, S. Kang, K.R. Ryu, G. Song, Real-time occupancy prediction in a large exhibition hall using deep learning approach, Energy Build. 199 (2019) 216–222.
[24] E.J. Choi, Y. Yoo, B.R. Park, Y.J. Choi, J.W. Moon, Development of occupant pose classification model using deep neural network for personalized thermal conditioning, Energies 13 (1) (2020).
[25] C. Zhong, J.H. Choi, Development of a data-driven approach for human-based environmental control, Procedia Eng. 205 (2017) 1665–1671.
[26] J.H. Choi, V. Loftness, Investigation of human body skin temperatures as a bio-signal to indicate overall thermal sensations, Build. Environ. 58 (2012) 258–269.
[27] J.S. Liu, I.W. Foged, T.B. Moeslund, Automatic estimation of clothing insulation rate and metabolic rate for dynamic thermal comfort assessment, Pattern Anal. Appl. 25 (3) (2022) 619–634.
[28] B. Gunay, Z. Nagy, C. Miller, M. Ouf, B. Dong, Using occupant-centric control for commercial HVAC systems, ASHRAE J. 63 (2021) 30–40.
[29] ISO 9920:2007, Ergonomics of the Thermal Environment — Estimation of Thermal Insulation and Water Vapour Resistance of a Clothing Ensemble, 2007. Switzerland.
[30] Y. Tang, Z.X. Su, H. Yu, K.G. Zhang, C.E. Li, H. Ye, A database of clothing overall and local insulation and prediction models for estimating ensembles' insulation, Build. Environ. 207 (2022).
[31] ISO 15831:2004, Clothing — Physiological Effects — Measurement of Thermal Insulation by Means of a Thermal Manikin, ISO, Switzerland, 2004.
[32] W.T. Sung, S.J. Hsiao, The application of thermal comfort control based on Smart House System of IoT, Measurement 149 (2020).
[33] F. Haldi, D. Robinson, Modelling occupants' personal characteristics for thermal comfort prediction, Int. J. Biometeorol. 55 (5) (2011) 681–694.
[34] M. Taleghani, M. Tenpierik, S. Kurvers, A. van den Dobbelsteen, A review into thermal comfort in buildings, Renew. Sustain. Energy Rev. 26 (2013) 201–215.

[35] P.M. de Carvalho, M.G. da Silva, J.E. Ramos, Influence of weather and indoor climate on clothing of occupants in naturally ventilated school buildings, Build. Environ. 59 (2013) 38–46.
[36] S. Schiavon, K.H. Lee, Dynamic predictive clothing insulation models based on outdoor air and indoor operative temperatures, Build. Environ. 59 (2013) 250–260.
[37] K.H. Lee, S. Schiavon, Influence of three dynamic predictive clothing insulation models on building energy use, HVAC sizing and thermal comfort, Energies 7 (4) (2014) 1917–1934.
[38] J. Miura, M. Demura, K. Nishi, S. Oishi, Thermal comfort measurement using thermal-depth images for robotic monitoring, Pattern Recogn. Lett. 137 (2020) 108–113.
[39] J.H. Lee, Y.K. Kim, K.S. Kim, S. Kim, Estimating clothing thermal insulation using an infrared camera, Sens.-Basel 16 (3) (2016).
[40] H. Choi, H. Na, T. Kim, T. Kim, Vision-based estimation of clothing insulation for building control: a case study of residential buildings, Build. Environ. 202 (2021).
[41] H. Matsumoto, Y. Iwai, H. Ishiguro, Estimation of Thermal Comfort by Measuring Clo Value without Contact, MVA, Citeseer, 2011, pp. 491–494.
[42] J. Dziedzic, D. Yan, V. Novakovic, Measurement of Dynamic Clothing Factor (D-CLO), NTNU, Trondheim, 2018.
[43] X.B. Xu, W.W. Liu, Z.W. Lian, Dynamic indoor comfort temperature settings based on the variation in clothing insulation and its energy-saving potential for an air-conditioning system, Energy Build. 220 (2020).
[44] M. De Carli, B.W. Olesen, A. Zarrella, R. Zecchin, People's clothing behaviour according to external weather and indoor environment, Build. Environ. 42 (12) (2007) 3965–3973.
[45] G.R. Newsham, Clothing as a thermal comfort moderator and the effect on energy consumption, Energy Build. 26 (3) (1997) 283–291.
[46] B.R. Park, E.J. Choi, Y.J. Choi, J.W. Moon, Development an image recognition-based clothing estimation model for comfortable building thermal controls, J. Architect. Inst. Korea 38 (1) (2022).
[47] G. Jocher, K. Nishimura, T. Mineeva, R. Vilarino, YOLOv5, 2020. https://ultralytics.com/yolov5, 05.
[48] E. McCullough, A data base for determining the evaporative resistance of clothing, Ashrae Trans. 95 (1989) 316–328.
[49] W.A. Lotens, G. Havenith, Effects of moisture absorption in clothing on the human heat-balance, Ergonomics 38 (6) (1995) 1092–1113.
[50] C. Zhong, J.H. Choi, Development of a data-driven approach for human-based environmental control, in: 10th International Symposium on Heating, Ventilation and Air Conditioning (ISHVAC), 2017, pp. 1665–1671. Jinan, PEOPLES R CHINA.
[51] P.M. Ferreira, A.E. Ruano, S. Silva, E.Z.E. Conceicao, Neural networks based predictive control for thermal comfort and energy savings in public buildings, Energy Build. 55 (2012) 238–251.
[52] K.A.f.T.a. Standards, KS C 9306, 2017, 2017.
[53] H.K. Kondaveeti, N.K. Kumaravelu, S.D. Vanambathina, S.E. Mathe, S. Vappangi, A systematic literature review on prototyping with Arduino: applications, challenges, advantages, and limitations, Comput. Sci. Rev. 40 (2021).
[54] J. Chandramohan, R. Nagarajan, K. Satheeshkumar, N. Ajithkumar, P.A. Gopinath, S. Ranjithkumar, Intelligent smart home automation and security system using Arduino and Wi-fi, Int. J. Eng. Comput. Sci.(IJECS) 6 (3) (2017) 4.
[55] C.R. Ruivo, M.G. da Silva, E.E. Broday, Methodology for calculating an atmospheric pressure-sensitive thermal comfort index PMVaps, Energy Build. 240 (2021).
[56] C.R. Ruivo, M.G. da Silva, E.E. Broday, Study on thermal comfort by using an atmospheric pressure dependent predicted mean vote index, Build. Environ. 206 (2021).